Establishing multiple osteogenic differentiation pathways of mesenchymal stem cells through different scaffold configurations

Running title – Scaffold configurations for osteogenic differentiation of stem cells

Salima Nedjari[1,2], Firas Awaja[1,3,4], Roberto Guarino[5], Dencho Gugutkov[1], George Altankov[1,6,7,*]

[1] *Institute for Bioengineering of Catalonia (IBEC), Barcelona, Spain*

[2] *Present address: Swiss Federal Laboratories for Materials Science and Technology EMPA, Laboratory for Biomimetic Membranes and Textiles, St.Gallen, Switzerland*

[3] *Engmat Ltd., Clybaun Road, Galway, Ireland*

[4] *Present address: Biomaterials & Tissue Engineering Lab, Experimental Orthopaedics, Department of Orthopaedic Surgery, Medical University Innsbruck, Innrain 36, Innsbruck, Austria*

[5] *École Polytechnique Fédérale de Lausanne (EPFL), Swiss Plasma Center (SPC), CH-5232 Villigen PSI, Switzerland*

[6] *ICREA (Institucio Catalana de Recerca i Estudis Avançats), Barcelona, Spain*

[7] Present address: Associate Member of the Institute of Biophysics and Biomedical Engineering, Bulgarian Academy of Sciences, Sofia, Bulgaria

*Corresponding author: altankov@abv.bg

ABSTRACT

Mimicking the complex organization of the extracellular matrix (ECM), especially structure and dimensionality, is necessary to produce living tissues from stem cells. In compliance with a previously-established role of nanofiber organization for the osteogenic differentiation of stem cells, here we used hybrid fibrinogen/poly(L-lactide-ε-caprolactone) (FBG/PLCL) nanofibers arranged in aligned and honeycomb configuration to recapitulate the highly oriented ECM of the cortical bone and the sponge-like (honeycomb) environment of the cancellous one, respectively. Using special bi-layered constructs, we demonstrate that the dimensionality (i.e., 2D *vs.* 3D) of the nanofibers as well as their architecture (i.e., honeycomb vs. aligned) affects differently the overall morphology and the multiple osteogenic genes expression of human adipose-derived mesenchymal stem cells (ADMSCs). The cells had elongated shape with markedly increased cell mobility when seeded on aligned nanofibers. Conversely, on honeycomb shaped fibers, ADMSCs initially concentrated inside the honeycomb curvatures adopting rounded morphology, but later they formed network-like structures overlaying the honeycomb curvatures. By employing quantitative polymerase chain reaction (qPCR), we further showed that a 3D environment generally supported the multiple osteogenic response of ADMSCs, but honeycomb and aligned architectures promoted rather different differentiation pathways.

KEYWORDS

Gel-nanofiber construct; honeycomb; aligned; stem cells; electrospinning; osteogenic differentiation; scaffolds.

INTRODUCTION

The worldwide incidences of bone disorders steeply increased and are expected to double by 2020, especially in populations where ageing is coupled with increased obesity and poor physical activity (Amini et al., 2012). Recently, engineered bone tissues have received great interest as potential alternatives to the conventional use of bone grafts, due to their limitless supply and the lack of disease transmission. However, bone tissue engineering (BTE) has not proceeded to clinical practices due to several limitations, including the insufficient differentiation and often tendency for de-differentiation of the osteogenic cells coming from a generally limited knowledge regarding the natural conditions that guide bone formation (Sagado et al., 2004).

Mesenchymal stem cells (MSCs) have long been recognized for their potential use in BTE because they differentiate and form bone during the natural bone development process. Their great potential in BTE has led to the characterization and identification of different sources for their isolation (Hass et al., 2011). The adipose-derived mesenchymal stem cells (ADMSCs) attract as an easily accessible and abundant source of autologous cells having multi-lineage differentiation potential, including osteogenic, chondrogenic, adipogenic, neural, cardiomyocyte, and endothelial lineages (Zuk et al., 2001; Planat-Benard et al., 2004). Moreover, lipoaspirates contain relatively large amounts of ADMSCs (e.g., from 1 to 5% of isolated cells) compared, for instance, to those in the bone marrow (e.g., from 0.001 to 0.1% of isolated cells) (Zuk et al., 2001).

Taking into account the significance of the cell microenvironment on the functionality of bone substitutes, the possibility of customizing 3D structured scaffold, able to support the cellular differentiation and functionality, becomes extremely important. The geometrical attributes of cellular interactions are key parameters for the success of implants (Amini et al., 2012). However, this remain an endearing task as most of the ECM fibrils exhibit well defined patterns and specific spatial orientations.

It is well known that the 3D structure of the natural bones is very complex and is not all solid. Mature bone is composed of about 40% extra-cellular matrix (ECM) formed before the mineral is deposited, thus it can be considered as natural a scaffold for the bone progenitor cells. About 90% of the bone ECM is composed of fibrillary collagen, whose linear triple helical molecules bond together into fibrils. The distinct organizational features, or cues, are strongly influential in directing cells behavior and functionality. Thus, the alignment between cells and fibrils is often considered as an important organizational cue (Clark et al., 1987). Particular alignment patterns of ECM and cells are observed in many tissues and organs, such as the corneal stroma, vascular smooth muscle cells, tendons and skeletal muscles (Bourget et al., 2013). Likewise the alignment is found also in the natural bone ECM (Clarke, 2008). It has to be also considered, however, that bone has generally anisotropic mechanical properties. The highly-oriented ECM with bone cells is characteristic rather for the cortical bone (Wang et al., 2013) and determine its unique tensile strength (Reilly et al., 1974). The cancellous bone is made of a sponge-like scaffold resembling a honeycomb structure (Clarke, 2008; Singh, 1978), resulting in the extremely high resistance of bone to compression (Gibson, 1985). The honeycomb structure, in addition to making bone more stable, represents an extremely efficient configuration because it is characterized by a very small amount matter per volume (i.e., material density). Thus, one can assume the existence of two main architectural cues within the bone ECM, characterized by linear and honeycomb organization, whose impact on the stem cells behavior is largely unknown.

The dimensionality is also a physical cue that drives stem cell differentiation. For example, concave and convex structures were found to influence strongly the osteogenic response of stem cells (Werner et al., 2017). Concerning the scaffolds, however, it is not trivial to recreate the highly organized 3D ECM microenvironment. The use of nanofibers has greatly improved the scope for preparing osteo-inductive scaffolds that resemble the architecture of the natural bone ECM at the nanoscale (Vasita et al., 2006). Given that electrospinning is a versatile technique to produce ECM like nanofibers, many efforts, including our previous work (Gugutkov et al., 2016), have been made for the synthesis with different geometries (e.g., random and aligned nanofibers) applicable to bone tissue

engineering (Cai et al., 2012; Jose et al., 2009). However, by modifying the casting parameters, it is also possible to produce more complex architectures, as the honeycomb one which, as described previously (Nedjari et al., 2014), provides more complex organization of the nanofibers layer in the out-of-plane direction.

Our recent paper (Nedjari et al., 2017) described in comparative plan the topographical response of ADMSCs to the organization of electrospun nanofibers, deposited as random, aligned and honeycomb-architectured scaffolds, showing for the first time a strong osteogenic response of stem cells on honeycomb-arranged nanofibers. This study however targeted the response of ADMSCs on nanofibers that are arranged in 2D geometries. Here, we continue this investigation by focusing specifically on the bioinspired configurations of aligned and honeycomb samples, now settled in a 3D environment that recapitulates to our view the highly-oriented ECM of the cortical bone and the honeycomb-like organization of the cancellous bone, respectively. We elaborated a special system that characterizes the particular role of the nanofibers dimensionality (i.e., 2D *vs.* 3D) using special gel-nanofiber constructs (Gugutkov et al., 2017) providing for culturing of cells in both plane (i.e., 2D) and sandwich-like (i.e., 3D) configurations. The biological response of stem cells was determined by the expression of multiple osteogenic genes *via* quantitative polymerase chain reaction (qPCR).

MATERIALS AND METHODS

Electrospinning of FBG-PLCL nanofibers

PLCL poly (L-lactide-ε-caprolactone) (70/ 30) (L-lactide/ε-caprolactone) was purchased from Corbion NV (Netherlands). Fibrinogen from bovine plasma and 1-1-1, 3-3-3-hexafluoroisopropanol (HFIP) was provided by Sigma Aldrich Inc. (United States of America). PLCL was dissolved in HFIP at a concentration of 12% wt/V for 24 hours prior to electrospinning. Fibrinogen (FBG) was dissolved at 100 mg mL^{-1} in HFIP mixed (9: 1) with 10× concentrated DMEM (Invitrogen, Thermo Fisher Scientific Inc., United States of America). The obtained FBG solution was cleared by centrifugation at 4000 rpm for 10 minutes. For the electrospinning, we used a tailor-made setup based on a high-voltage power supply (Glassman High Voltage Inc., United States of America), a syringe pump (Aitecs, Viltechmeda UAB, Lithuania), and a grounded collector all fitted in a plastic chamber. PLCL and FBG were mixed in 1:1 ratio and loaded in a conventional 10 mL syringe (BD Biosciences, United States of America). The pump flow rate was 0.6 mL h^{-1}. The applied voltage was 20 kV, the distance between the needle tip and the collector was 13 cm.

Fiber Morphology and alignment

The morphology of nanofibers was observed by scanning electron microscopy (SEM) using a Nova NanoSem 230 (FEI, Thermo Fisher Scientific Inc., United States of America) at a voltage of 5 kV. The samples were coated with a conductive layer of sputtered gold (10 nm) prior to observations with the SEM.

Preparation of the Biocompatible Hydrogel

Biocompatible hydrogel discs were used to deposit nanofibers and to arrange 3D constructs. They were produced according to a previously described protocol (Gugutkov et al., 2017) and designed to fit to the 48 well tissue culture plates (Nunc AS, Denmark).

Cells

Human ADMSCs were obtained from Lonza BioWhittaker (Lonza Group, Belgium). The cells were seeded in 75 cm^2 flasks and expanded in DMEM/F12 (1:1) supplemented with 1% GlutaMAX™, 1 % Antibiotic-Antimycotic solution supplemented with 10% Fetal Bovine Serum (FBS) in humidified CO_2 incubator at 37 °C. The medium was replaced every 2 days.

Preparation of 2D nanofibrous samples

The honeycomb scaffolds were synthesized using honeycomb shaped collector produced by photolithography on silicon wafers (MJB4, SÜSS MicroTect SE, Germany). The photoresist used was SU-8 2050 (Microchem). A Univex 450B (Oerlikon Leybold Vaccum GmbH) electron beam evaporator was used to deposit a conductive layer (150 nm-thick Au) on the collectors. The collector had an internal diameter of 160 µm. The width and the height of the honeycomb walls were 20 and 60 µm, respectively. After electrospinning, the resulting membrane was peeled off from the collector, punched to obtain honeycomb samples with a diameter of 12 mm, and attached to the gels by capillarity, resulting in the formation of the hybrid gel-nanofiber honeycomb architecture.

Aligned fibers were produced using the same electrospinning conditions, but using a previously-described method[30]. Briefly, two plastic discs, with a diameter of 120 mm, were mounted on a common axis separated at a 100 mm distance. Thin metal wires were stretched between the discs peripheries to form parallel strings with a 16 mm separation. While rotating the common axis at 600-800 rpm, the nanofibers aligned between the metal wires were collected onto the gels. Gels covered by the fibers were the 2D construct.

Preparation of the 3D constructs

Early passage human ADMSCs (up to the 4^{th} passage) were harvested with Tripsin/EDTA and seeded onto the 2D gel-supported nanofiber scaffolds, as described above, at a density of $2 \cdot 10^4$ cells per sample. The cell-loaded samples were further cultured for 3-5 days in DMEM supplemented with

10% FBS before being switched to osteogenic differentiation conditions (see below) under 2D or 3D environment.

For the creation of the 3D environment, sandwich-like constructs were assembled via joining two cell-loaded samples facing each other with their cellular site, taking special care to put aligned samples in the same direction.

Overall cell morphology and visualization of focal adhesion complexes

The overall morphology of ADMSC cultured on 2D aligned and honeycomb PLCL/FBG scaffolds was evaluated after 5 hours, 1 day, and 6 days of incubation. To follow the focal adhesion formation and actin cytoskeleton reorganization, fixed samples were permeabilized with 0.5% Triton-X 100 (Sigma-Aldrich) and saturated with 1% BSA for 20 minutes to avoid unspecific binding before stained with a monoclonal anti-vinculin antibody (Sigma-Aldrich, V9264) (dilution 1:800) for 30 minutes at 37°C. The samples were stained by goat anti-mouse IgG AlexaFluor 555-conjugated secondary antibody (Life Technologies, A11001) supplemented with Hoechst (dilution 1:500, Invitrogen) and FITC Phalloidin (Invitrogen 34580) for 30 minutes at 37 °C, for simultaneous staining of the cell nuclei and actin cytoskeleton, respectively. At least three representative images were acquired for each sample at low magnification (i.e., 10X) for the overall morphology and at high magnification (i.e., 63X) to observe the focal adhesions and cytoskeleton organization.

Osteogenic response of ADMSCs

Once the confluency of ADMSCs was reached (at day 5-6) the second part of the experiment was started, i.e., the comparative analysis of the osteogenic differentiation of stem cells in 2D and 3D environment employing specifically designed gel-nanofiber constructs (see above). Therefore, the media in the 48 TC plates (containing the constructs) was changed from the proliferative to osteogenic induction medium consisted of DMEM supplemented with 100 nM dexamethasone, 50 µM l-ascorbate-2-phosphate and 10 mM β-glycerophosphate and further cultured up to 21 day. The culture medium was replaced every 2 days.

Real-time PCR

The osteogenic differentiation of ADMSCs was followed by quantitative relative time PCR. Total cellular RNA was extracted from the middle tissue discs by using RNeasy Mini Kit (QIAGEN, Germany). Reverse transcription was performed by processing of 10 µL of three times diluted RNA-eluate with High Capacity cDNA Reverse Transcription Kit (Applied Biosystems) according to the suppliers protocol. Quantitative PCR analysis (qPCR) of the gene expression was carried out with fast real-time PCR System (Applied Biosystems 7900HT). Briefly, a single qPCR reaction consisted of mixing 10 µL Taqman Gene Expression Master Mix (Applied Biosystems), 1 µL TaqMan primers (Applied Biosystems), 5 µL nuclease-free H2O and 4 µL of sample cDNA. TaqMan primers used for the detection of osteogenic differentiation are the following: RunX2 (Primer:Hs01047973_m1), Osterix (Primer:Hs00541729_m1), Bone Sialioprotein (Primer:Hs00173720_m1) and Osteocalcin (Primer: Hs01587814_g1). GAPDH (Primer: Hs02758991_g1) was used as housekeeping gene.

Each sample was run in triplicate and the cycling program was set on 95° C for 10 min, followed by 40 cycles of 95 °C for 15 s, and 60 °C for 1 min. Data analysis was performed by DataAssist Software (Thermo Fisher Scientific, Spain). Comparative CT analysis was used to determine the relative expression of each target gene. The amount of the target gene was normalized to GAPDH as housekeeping gene. Transcription levels were expressed as fold change from the calibrator control value. Non-stimulated confluent ADMSCs were used as a control in all qPCR experiments.

Statistical analysis

Data from all quantitative analysis were expressed as mean ± standard deviation and subjected to a one-way ANOVA variance analysis. Each experiment was performed in triplicates and repeated at least twice. Statistical significance was determined by Student's t-test. Probability values with $p < 0.05$ were considered as statistically significant.

RESULTS

In this study we aimed to establish the biological response of ADMSCs on two biomimetic scaffolds with distinct architectures, i.e., aligned and honeycomb, arranged in a 3D configuration to better mimic the organization of ECM in the cortical and cancellous bone, respectively. For the production of nanofibers we utilized two previously described electrospinning protocols (Nedjari et al., 2014; Gugutkov et al., 2016) with some specific modifications, as detailed below. We further followed the expression of different osteogenic markers using specially designed constructs, in order to better allow a comparison between the 2D and 3D environments. For this study, we were motivated from our previous observations showing that honeycomb scaffolds strongly support the osteogenic response of osteoblasts (Nedjari et al., 2017) and ADMSCs (Gugutkov et al., 2017) in 2D environments, and also from another previous study demonstrating the beneficial effects of aligned nanofiber orientation with respect to the random ones (Gugutkov et al., 2017). In the same previous work (Nedjari et al., 2017), we employed Alizarin Red and Von Kossa staining to analyze the hydroxyapatite formation on honeycomb and aligned electrospun PLCL-FBG scaffolds, demonstrating a significantly increased production of hydroxyapatite on honeycomb scaffolds (in 2D systems). Here, instead, the focus is on the difference between the 2D and the 3D environment. The comparative aspects of these architectures and the particular role of nanofibers dimensionality, in fact, were not clearly addressed until now.

For this study we employed recently described hybrid nanofibers (Nedjari et al., 2017) based on fibrinogen (FBG) and poly(L-lactide- ε-caprolactone) (PLCL), considering that FBG allows a natural cell recognition. It has to be noted that, apart from its well-known role in the coagulation cascade (Lisman et al., 2005) and wound healing (Raghow, 1994), FBG is also a naturally-occurring ECM protein in some tissues like lung and intestinum (Pereira et al., 2002). On the other hand, inclusion of PLCL significantly improve the nanofibers mechanical properties, keeping the bioactivity of FBG unaltered (Gugutkov et al., 2016). For the production of scaffolds with honeycomb architecture we used a

specially-designed honeycomb-shaped collector prepared by photolithography (Nedjari et al., 2014; Nedjari et al., 2017). Aligned scaffolds were produced also using the original technique described previously (Gugutkov et al., 2016) (see Materials and Methods Section).

Figure 1 shows the SEM and immunofluorescence images of the nanofibers on aligned and honeycomb-shaped scaffolds. We decided to acquire the pictures only within 24 h after cell seeding, since, to our experience, the accumulating ECM and the covering by fibers makes them not clear at later stages.

Comparing the overall morphology of aligned (Figure 1A) and honeycomb samples (Figure 1B), we found that nanofibers preferentially deposited on the top of the honeycomb patterns presumably due to stronger electrostatic field accumulating there (Nedjari et al., 2014). Further analysis of the SEM images from these samples showed that fibers on the honeycomb scaffolds present bimodal size distribution consisting of thin fibers with main diameter of 195 ($\pm$ 50) nm, and thick ones of 462 ($\pm$117) nm. For the aligned samples the distribution was 195 ($\pm$63) nm and 491 ($\pm$ 182) nm, respectively. For details about the observed fiber distributions, the reader is referred to our previous work (Nedjari et al., 2017).

We also observed that the honeycomb walls were formed predominantly from thick fibers, while mostly thinner ones formed the bottom of the honeycomb niches. The presence of FBG within the fibers was confirmed by immunostaining and, as shown in Figures 1C and 1D, the walls of the honeycombs, having height of about 10 μm, showed much stronger accumulation of FBG, presumably due to the higher density of the fibers. In this work, we present morphological information to show the behavior of ADMSCs in a 2D environment. To get comparative images from the 3D constructs (the main target of this paper) was complex. All attempts to get orthogonal views from reconstructed 3D confocal images of the cell layers (stained for actin) were futile because of the high background of the samples.

The overall morphology of adhering ADMSCs followed on the planar 2D scaffolds was also affected by the substratum geometry. On aligned nanofibers, the cells showed extended morphology (Figure 1E) with stretched actin filaments following the directions of nanofibers. This process visibly progressed after 24 hours of culture (Figure 1G). Interestingly, on honeycomb shaped fibers, the cells initially concentrated inside the honeycomb compartments adopting a rather rounded morphology, characteristic for the cells in a 3D environment (Figure 1F). It has to be noted however that the honeycomb arrangement is not a really "true" 2D environment as the honeycomb invaginations have nearly of the same cell size, so cells seeded there will experience also lateral signals. In fact, honeycomb compartments represent a nearly 3D environment, though not complete (some authors refer it as 2.5D environment) as cells miss the signals from the top. Nevertheless, it is sufficient to influence significantly their initial morphology. On the next day however, the stem cells started to organize in network-like structures overlaying the honeycombs (Figure 1H), forming actually a rather 2D layer. Apparently, before forming networks, the cells moved first to the top of the walls and then link each other over the honeycombs. The affinity of cells to move top-hill we suppose is due to the predominant accumulation of FBG on those sites.

Cell proliferation was assessed in our previously published papers utilizing electrospun PLCL-FBG scaffolds (Nedjari et al., 2017; Gugutkov et al., 2017), showing no cytotoxic effects in both 2D and 3D cell culture systems.

To follow the osteogenic differentiation in 3D environment, we applied a special gel-nanofibrous construct (Gugutkov et al., 2017), where ADMSCs were cultured in either planar (i.e., 2D) or sandwich-like configuration (i.e., 3D). qPCR was used to detect the activity of osteogenic markers RUNX2, osterix (OST), bone sialoprotein (BSPII), and osteocalcin (OCN). The overall design of the experiment is schematized in Figure 2.

Hybrid scaffolds consisting of aligned and honeycomb nanofibers deposited on a biocompatible gel provided for further arrangement in a planar (2D) or 3D sandwich-like configuration (Gugutkov et al., 2017). Early-passage human ADSMCs were first seeded onto aligned or honeycomb samples in 2D configuration and cultured for 3-5 days until rich confluence. One part of these 2D samples were then assembled together in a sandwich-like configuration, with the cellular layers facing each other, while the rest was left as controls. Then the resulting 2D and 3D constructs were cultured for 21 days in an osteogenic medium.

The qPCR results are presented on Figure 3 showing the expression of two transcription factors, i.e., RUNX2 and OST, and two matrix protein-related genes, i.e., BSP and OCN. Since the osteogenic response of ADMSCs is usually maximal after 3 weeks of culture, we decided to perform qPCR only at the day 21. This choice allowed to maximize the osteogenic response and thus to better focus on the main scope of the analysis, i.e., the comparison between the 2D and the 3D environments. The observed heterogeneous expression of these markers provides insights on the activation of different osteogenic programs of ADMSCs, as detailed in the discussion below. In this study we found that the activation of different markers at different levels of differentiation between honeycomb and aligned environments, also between 2D and 3D systems deserved our focused attention. Some of the assays were not possible to conduct in the 3D environment of constructs that prevented the comparison with the corresponding 2D samples. The proteomics and functional tests on the osteogenic response of ADMSCs (such as alkaline phosphatase activity, fibronectin matrix synthesis, Ca deposition, focal adhesions formation, etc.) were already reported in our previous work (Nedjari et al., 2017), and hence have not been repeated here.

DISCUSSION

The observed morphological effects are extremely relevant, considering the number of recent studies showing that the initial shape of stem cells plays a substantial role in the initiation of their osteochondral program (Nedjari et al., 2017). Prior to condensation, stem cells express a typical mesenchymal morphology, which changes after increasing their homotypic contacts, thus losing the substratum dependence (DeLise et al., 2000). Other studies highlight that mesenchymal stem cells need close contacts in the niche to start differentiation (Li et al., 2005). Interestingly, such tendency was observed also in our honeycomb microenvironment, where ADMSCs tended to form network-like structures, suggesting an increase of intercellular adhesions; a behavior not seen in the aligned samples. It appears that the honeycomb shape provokes specifically the homotypic cell interaction, presumably as an attempt to bridge, or to overcome, the honeycomb curvature.

The heterogeneous expression of osteogenic markers, observed through qPCR, demonstrates the activation of different osteogenic programs of ADMSCs.

First, to interpret the result on RUNX2 expression (Figure 3A), we have to consider that this gene activity is related to the synthesis of a transcription factor that promotes osteoblast differentiation at the early stage of osteogenesis. This plays a crucial role in the determination of an osteoblastic lineage from the mesenchymal stem cells. Our results primarily indicate a better expression of RUNX2 in the 3D than in the 2D environment. The activity of the honeycomb architecture however significantly override those of aligned scaffolds. Komori showed that RUNX2-deficient mice exhibit a complete lack of bone formation (i.e., no endochondral and intramembranous ossification) due to the absence of osteoblasts (Komori, 2009), demonstrating the important role of this transcription factor. Thus, our results demonstrate that the honeycomb geometry may promote the initial osteoblasts generation, mimicking the condensation step of physiological osteogenesis. This view is supported by our morphological observations (performed in 2D conditions), suggesting prevailing homotypic adhesions within the cellular network observed on honeycomb scaffolds. Conversely, highly aligned nanofibers

provide less probability for cell-cell contacts, as seen in 2D conditions. The 3D environment however may disguise this effect (Figure 3A). Nevertheless, the RUNX2 activity on all aligned constructs still show values that significantly override the basic ADMSCs activity, meaning that both geometries are favourable for the osteoblasts maturation from stem cells.

Figure 3B shows the data for OST expression, which is another transcriptional factor, essential for the differentiation of pre-osteoblasts into functional osteoblasts (Nakashima et al., 2002). OST activity also shows clear response to the 3D environment for both architectures, with an increase of about 30% with respect to the 2D samples. The expression of OST however is significantly lowered in ADMSCs cultured on honeycomb scaffolds, showing values close to the basic ADMSCs activity. Extrapolating these data to the physiological condition *in vivo*, we speculate that the cellular transition from pre-osteoblast to functional osteoblasts might be lowered in the relatively static (honeycomb-like) environment of the cancellous bone. Conversely, the aligned environment, such as the highly oriented osteoid matrix of the cortical bone, may actively supports the endochondral bone formation working downstream RUNX2 (Sinha et al., 2013). The importance of this transcription factor is highlighted in a study showing that mice lacking OST die within an hour of birth with a complete absence of endochondral bone formation (Baek et al., 2009). When OST is inactivated in adult mice, however, no abnormality was detected at birth. But later, these mice developed osteopenia (i.e., a thinner and more porous cortical bone) while no morphological alterations in the cancellous bone were detected (Baek et al., 2009). Turning to the *in vivo* conditions, the key role of OST in the formation of long bones is connected to the cortical bone activity, but it is rather downregulated in the honeycomb-like environment of the cancellous bone.

Apart from OST, the expression of BSP gene was strongly increased by the honeycomb geometry (Figure 3C), particularly in 3D conditions, where it significantly override the basic ADMSCs activity. In order to better understand this point, we briefly summarize the physiological role of this protein. BSP is abundantly expressed in all bone tissues comprising about 15% of the total non-collagenous protein (Wuttke et al., 2001) and both osteoblasts and osteocytes secrete it (Ganss et al., 1999). During bone

formation, the osteoblasts first deposit a non-mineralized osteoid matrix consisting mostly of collagen fibrils (Jäger et al., 2000), which subsequently is mineralized by incorporation of carbonated hydroxyapatite (HA). Bone mineralization process as a whole is not well understood, however, it is clearly documented that the HA crystals deposits preferentially within the collagen fibers (i.e., in the gap regions) (White et al., 1977) tending to orient with their c-axes parallel to the long axis of the collagen fibrils (Stühler, 1937). Therefore, it is widely accepted that collagen provoke HA uptake, though collagen itself is known as a slow initiator of mineralization (Glimcher, 1989). Malaval *et al.* showed that mice lacking BSP gene have reduced size of long bones suggesting the induction of bone resorption (Malaval et al., 2008). On the other hand, BSP is a typical RGD-containing protein that mediates integrin binding and cell adhesion (Roach, 1994), thus it recruit osteoclasts to the bone matrix. In agreement with this, Wuttke *et al.* demonstrated that BSP promotes bone resorption in a concentration-dependent manner (Wuttke et al., 2001). That is to say that BSP has strong impact on the endochondral ossification having double role in both, mineralization and resorption, i.e., supporting bone remodeling. Despite it was suggested that the BSP has no major, but rather redundant function in mature bone (Malaval et al., 2008), we speculate that its significant expression in the honeycomb architecture means that it favors the natural bone remodeling responsible for the shaping of cancellous bone.

With reference to the OCN gene activity, our results show that it is more evident on aligned scaffolds in both 2D and 3D conditions, while honeycomb scaffolds surprisingly exhibit only a negligible expression, close to the basic activity of ADMSCs. OCN is a low molecular weight matrix protein (5800 Da), physiologically connected with the late stages of mineralization (Bronckers et al., 1985). In humans, the cortical bone contains 30 times more OCN then the cancellous one (Ninomiya et al., 1990), which to our view correlates well with its stronger expression on aligned scaffolds. The reason for the lack of OCN gene expression on honeycomb scaffold remains unclear, keeping in mind our recent study comparing aligned and honeycomb scaffolds in 2D conditions demonstrating higher Ca deposition on the honeycomb ones (Nedjari et al., 2017). At this point it is worthy to mention a line of

research identifying osteocalcin as a negative regulator of bone formation, which to our view might be a “desirable” fit-back within the relatively static environment of the cancellous bone (Ducy et al., 1996). On the other hand, however, OCN is reported to regulate directly the mineralization of bone controlling the growth and the size of HA crystals (Roach, 1994). For example, no defects were observed at the birth in osteocalcin free mutant mice, but after 6 months an increased cortical thickness and density of the long bones was measured, suggesting a significant bone formation even though there was no increase in the number of osteoblasts. That is to say that the topical localizations of osteogenic progenitor cells may provoke or inhibit their functional response to OCN upon residing in differently arranged microenvironment.

CONCLUSIONS

Taken collectively, our results show that stem cell differentiation and bone remodeling are closely dependent on the overall architecture and the dimensionality of the surrounding matrix. 3D scaffolds generally support the osteogenic path of ADMSCs differentiation. However, the topical organization of nanofibers has also a strong impact, which can vary significantly between aligned and honeycomb scaffolds. The spatially oriented signals from the aligned FBG/PLCL nanofibers drive ADMSCs to differentiate quicker from pre-osteoblasts to mature osteoblasts, evident by stronger expressions of OST and OCN markers. Conversely, the honeycomb architecture supports rather the osteoblasts functionality and ECM remodeling, as suggested by the prevailing expression of RUNX2 and BSP markers. The highly interconnected cellular network observed morphologically in the 2D honeycomb scaffold is supposed to promotes ADMSCs differentiation into functional osteoblasts, because resembling the condensation step of bone maturation. The physiological weight of these complex biological events relates to the behavior of the stem cells within the highly-aligned architecture of cortical bone versus the relatively static honeycomb-like environment of cancellous bone.

The present results show that there is a significant difference between 2D and 3D environments, confirming our previous study that cells “sense” their counterparts from another layer (contacting each other directly or through their ECM) affecting their differentiation to chondrogenic lineage. The novelty of this work consists of establishing a system that compare the effects of two different bioinspired nanofibrous microenvironments on the osteogenic response of ADMSCs, i.e., aligned and honeycomb, now in 2D *vs.* 3D configuration. The qPCR data further show that nanofibers organization may affects different stages of stem cells osteogenic response, and this analysis represents an important added value to this work. Future research activities could be focused on the study of more complex 3D geometries, e.g., by making use of additive manufacturing techniques, and on verifying protein expression as a complementary tool to qPCR.

ACKNOWLEDGMENTS

This work was mainly supported by the European Commission through FP7 Industry-Academia Partnerships and Pathways (IAPP) project FIBROGELNET, coordinated by GA. The valuable contribution of project MAT 2015-69315-C3 MYOHEAL with the Spanish Ministry of Science and Innovation and CIBER-BBN are also acknowledged. FA acknowledges the partial support of FWF under Lise Meitner program (M-1777) and also of grant No 713690 provided by European Commission within the Horizon 2020 Marie Curie-Skłodowska program.

CONFLICT OF INTEREST STATEMENT

The authors declare the absence of any potential sources of conflict of interest.

REFERENCES

Amini, A. R.; Laurencin, C. T.; Nukavarapu, S. P. Bone. (2012). Tissue Engineering: Recent Advances and Challenges. Crit. Rev. Biomed. Eng. , 40. doi: 10.1615/critrevbiomedeng.v40.i5.10

Baek, W.; Lee, M.; Jung, J. W.; Kim, S.; Akiyama, H.; de Crombrugghe, B.; Kim, J. (2009). Positive Regulation of Adult Bone Formation by Osteoblast-specific Transcription Factor Osterix. J. Bone Miner. Res., 24, 1055–1065. doi: 10.1359/jbmr.081248

Bourget, J.-M.; Guillemette, M.; Veres, T.; Auger, F. A.; Germain, L. Alignment of Cells and Extracellular Matrix within Tissue-Engineered Substitutes. (2013). In *Advances in Biomaterials Science and Biomedical Applications*; InTech.

Bronckers, A. L. J. J.; Gay, S.; Dimuzio, M. T.; Butler, W. T. (1985). Immunolocalization of γ-Carboxyglutamic Acid Containing Proteins in Developing Rat Bones. Coll. Relat. Res., 5, 273–281. doi: 10.1016/s0174-173x(85)80017-0

Cai, Y.; Zhang, G.; Wang, L.; Jiang, Y.; Ouyang, H.; Zou, X. (2012). Novel Biodegradable Three-dimensional Macroporous Scaffold Using Aligned Electrospun Nanofibrous Yarns for Bone Tissue Engineering. J. Biomed. Mater. Res. Part A, 100, 1187–1194. doi: 10.1002/jbm.a.34063

Clark, P.; Connolly, P.; Curtis, A. S.; Dow, J. A.; Wilkinson, C. D. (1987). Topographical Control of Cell Behaviour. I. Simple Step Cues. Development, 99, 439–448.

Clarke, B. (2008). Normal Bone Anatomy and Physiology. Clin. J. Am. Soc. Nephrol., 3 (Supplement 3), S131–S139. doi: 10.2215/CJN.04151206

DeLise, A. M.; Fischer, L.; Tuan, R. S. (2000). Cellular Interactions and Signaling in Cartilage Development. Osteoarthr. Cartil., 8 (5), 309–334. doi: 10.1053/joca.1999.0306

Ducy, P.; Desbois, C.; Boyce, B.; Pinero, G.; Story, B.; Dunstan, C.; Smith, E.; Bonadio, J.; Goldstein, S.; Gundberg, C. (1996). Increased Bone Formation in Osteocalcin-Deficient Mice. Nature, 382, 448-452. doi: 10.1038/382448a0

Ganss, B.; Kim, R. H.; Sodek, J. (1999). Bone Sialoprotein. Crit. Rev. Oral Biol. Med., 10, 79–98. doi: 10.1177/10454411990100010401

Gibson, L. (1985). The Mechanical Behaviour of Cancellous Bone. *J. Biomech., 18*, 317–328. doi: 10.1016/0021-9290(85)90287-8

Glimcher, M. J. (1989). Mechanism of Calcification: Role of Collagen Fibrils and Collagen-phosphoprotein Complexes in Vitro and in Vivo. Anat. Rec., 224, 139–153. doi: 10.1002/ar.1092240205

Gugutkov, D.; Gustavsson, J.; Cantini, M.; Salmeron-Sánchez, M.; Altankov, G. (2016). Electrospun Fibrinogen–PLA Nanofibres for Vascular Tissue Engineering. J. Tissue Eng. Regen. Med. doi: 10.1002/term.2172

Gugutkov, D.; Awaja, F.; Belemezova, K.; Keremidarska, M.; Krasteva, N.; Kyurkchiev, S.; Gallego-Ferrer, G.; Seker, S.; Elçin, A. E.; Elçin, Y. M. (2017). Osteogenic Differentiation of Mesenchymal Stem Cells Using Hybrid Nanofibers with Different Configurations and Dimensionality. J. Biomed. Mater. Res. Part A, 105, 2065–2074. doi: 10.1002/jbm.a.36065

Hass, R.; Kasper, C.; Böhm, S.; Jacobs, R. (2011). Different Populations and Sources of Human Mesenchymal Stem Cells (MSC): A Comparison of Adult and Neonatal Tissue-Derived MSC. Cell Commun. Signal., 9, 12. doi: 10.1186/1478-811X-9-12

Jäger, I.; Fratzl, P. (2000). Mineralized Collagen Fibrils: A Mechanical Model with a Staggered Arrangement of Mineral Particles. Biophys. J., 79, 1737–1746. doi: 10.1016/S0006-3495(00)76426-5

Jose, M. V; Thomas, V.; Johnson, K. T.; Dean, D. R.; Nyairo, E. (2009). Aligned PLGA/HA Nanofibrous Nanocomposite Scaffolds for Bone Tissue Engineering. Acta Biomater., 5, 305–315. doi: 10.1016/j.actbio.2008.07.019

Komori, T. (2009). Regulation of Osteoblast Differentiation by Runx2. In *Osteoimmunology*; Springer; pp 43–49. doi: 10.1007/978-1-4419-1050-9_5

Li, L.; Xie, T. (2005). Stem Cell Niche: Structure and Function. *Annu. Rev. Cell Dev. Biol.*, *21*, 605–631. doi: 10.1146/annurev.cellbio.21.012704.131525

Lisman, T.; Weeterings, C.; de Groot, P. G. (2005). Platelet Aggregation: Involvement of Thrombin and Fibrin (Ogen). Front Biosci, 10, 2504–2517. doi: 10.2741/1715

Malaval, L.; Wade-Guéye, N. M.; Boudiffa, M.; Fei, J.; Zirngibl, R.; Chen, F.; Laroche, N.; Roux, J.-P.; Burt-Pichat, B.; Duboeuf, F. (2008). Bone Sialoprotein Plays a Functional Role in Bone Formation and Osteoclastogenesis. J. Exp. Med., 205, 1145–1153. doi: 10.1084/jem.20071294

Nakashima, K.; Zhou, X.; Kunkel, G.; Zhang, Z.; Deng, J. M.; Behringer, R. R.; de Crombrugghe, B. (2002). The Novel Zinc Finger-Containing Transcription Factor Osterix Is Required for Osteoblast Differentiation and Bone Formation. Cell, 108, 17–29. doi: 10.1016/s0092-8674(01)00622-5

Nedjari, S.; Eap, S.; Hébraud, A.; Wittmer, C. R.; Benkirane-Jessel, N.; Schlatter, G. (2014). Electrospun Honeycomb as Nests for Controlled Osteoblast Spatial Organization. Macromol. Biosci., 14, 1580–1589. doi: 10.1002/mabi.201400226

Nedjari, S.; Awaja, F.; Altankov, G. (2017). Three Dimensional Honeycomb Patterned Fibrinogen Based Nanofibers Induce Substantial Osteogenic Response of Mesenchymal Stem Cells. Sci. Rep., 7 (1). doi: 10.1038/s41598-017-15956-8

Pereira, M.; Rybarczyk, B. J.; Odrljin, T. M.; Hocking, D. C.; Sottile, J.; Simpson-Haidaris, P. J. (2002). The Incorporation of Fibrinogen into Extracellular Matrix Is Dependent on Active Assembly of a Fibronectin Matrix. J. Cell Sci., 115, 609–617.

Planat-Benard, V.; Menard, C.; André, M.; Puceat, M.; Perez, A.; Garcia-Verdugo, J.-M.; Pénicaud, L.; Casteilla, L. (2004). Spontaneous Cardiomyocyte Differentiation from Adipose Tissue Stroma Cells. Circ. Res., 94, 223–229. doi: 10.1161/01.RES.0000109792.43271.47

Raghow, R. (1994). The Role of Extracellular Matrix in Postinflammatory Wound Healing and Fibrosis. FASEB J., 8, 823–831. doi: 10.1096/fasebj.8.11.8070631

Reilly, D. T.; Burstein, A. H. (1974). The Mechanical Properties of Cortical Bone. JBJS, 56, 1001–1022.

Roach, H. I. (1994). Why does bone matrix contain non-collagenous proteins? The possible roles of osteocalcin, osteonectin, osteopontin and bone sialoprotein in bone mineralisation and resorption. Cell Biol. Int., 18, 617–628. doi: 10.1006/cbir.1994.1088

Salgado, A. J.; Coutinho, O. P.; Reis, R. L. (2004). Bone Tissue Engineering: State of the Art and Future Trends. Macromol. Biosci., 4, 743–765. doi: 10.1002/mabi.200400026

Sinha, K. M.; Zhou, X. (2013). Genetic and Molecular Control of Osterix in Skeletal Formation. J. Cell. Biochem., 114, 975–984. doi: 10.1002/jcb.24439

Singh, I. (1978). The Architecture of Cancellous Bone. J. Anat., 127, 305.

Stühler, R. (1937). Über Den Feinbau Des Knochens. Fortschr. Röntgenstr, 57, 231.

Vasita, R.; Katti, D. S. (2006). Nanofibers and Their Applications in Tissue Engineering. Int. J. Nanomedicine, 1, 15. doi: 10.2147/nano.2006.1.1.15

Wang, X.; Ding, B.; Li, B. (2013). Biomimetic Electrospun Nanofibrous Structures for Tissue Engineering. Mater. Today, 16, 229–241. doi: 10.1016/j.mattod.2013.06.005

Werner, M.; Blanquer, S. B. G.; Haimi, S. P.; Korus, G.; Dunlop, J. W. C.; Duda, G. N.; Grijpma, D.; Petersen, A. (2017). Surface Curvature Differentially Regulates Stem Cell Migration and Differentiation via Altered Attachment Morphology and Nuclear Deformation. *Adv. Sci., 4*. doi: 10.1002/advs.201770007

White, S. W.; Hulmes, D. J.; Miller, A.; Timmins, P. A. (1977). Collagen-Mineral Axial Relationship in Calcified Turkey Leg Tendon by X-Ray and Neutron Diffraction. Nature, 266, 421–425. doi: 10.1038/266421a0

Wolf, G. (1996). Function of the Bone Protein Osteocalcin: Definitive Evidence. Nutr. Rev., 54, 332–333. doi: 10.1111/j.1753-4887.1996.tb03798.x

Wuttke, M.; Müller, S.; Nitsche, D. P.; Paulsson, M.; Hanisch, F.-G.; Maurer, P. (2001). Structural Characterization of Human Recombinant and Bone-Derived Bone Sialoprotein Functional Implications for Cell Attachment and Hydroxyapatite Binding. J. Biol. Chem., 276, 36839–36848. doi: 10.1074/jbc.M105689200

Zuk, P. A.; Zhu, M.; Mizuno, H.; Huang, J.; Futrell, J. W.; Katz, A. J.; Benhaim, P.; Lorenz, H. P.; Hedrick, M. H. (2001). Multilineage Cells from Human Adipose Tissue: Implications for Cell-Based Therapies. Tissue Eng., 7, 211–228. doi: 10.1089/107632701300062859

FIGURE LEGENDS

Figure 1 - Overall morphology of architectured nanofibers and adhering cells.

Figure 2 - Schematic view of the overall design of experiments.

Figure 3 - Gene expression on the considered 2D and 3D constructs.

FIGURES

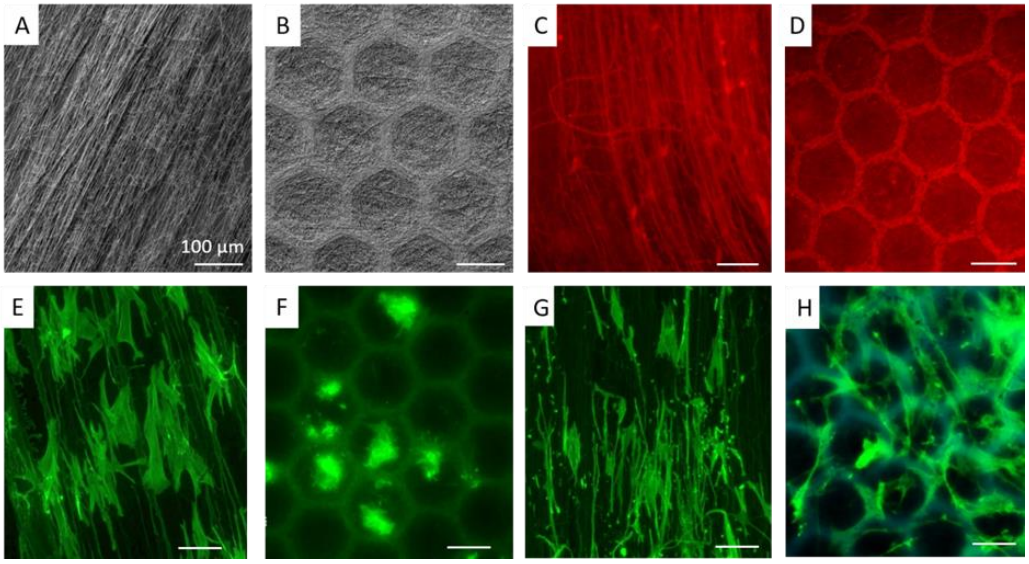

Figure 1. Overall morphology of architectured nanofibers and adhering cells.

SEM images of aligned (A) and honeycomb-shaped (B) PLCL-FBG nanofibers. Immunofluorescence visualization of fibrinogen within the fibers (red) in aligned (C) and honeycomb-shaped (D) scaffolds. Overall morphology of ADMSCs viewed for actin cytoskeleton (green) after 5 h of adhesion on aligned (E) and honeycomb-arranged (F) nanofibers. Cells morphology after 24 h of incubation on aligned (G) and honeycomb-shaped (H) scaffolds.

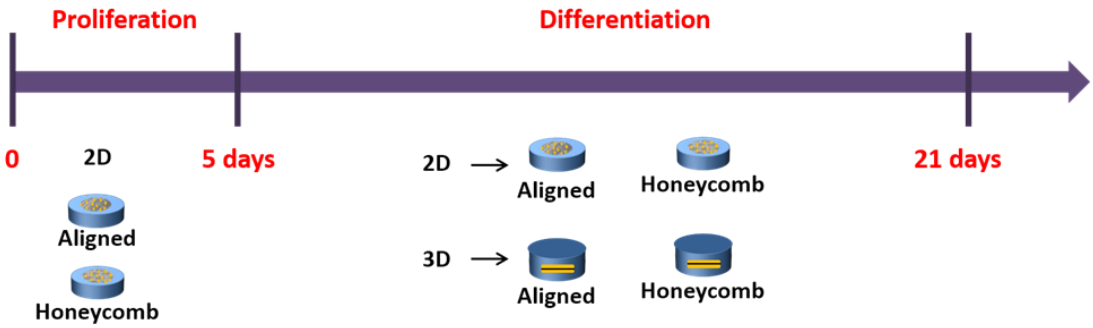

Figure 2. Schematic view of the overall design of experiments.

Assembly of 2D and 3D constructs consisting of aligned or honeycomb nanofibers and overall design of the experiments aimed at comparing the osteogenic response of ADMSCs in 2D and 3D environments. For each configuration, triplicate samples were examined.

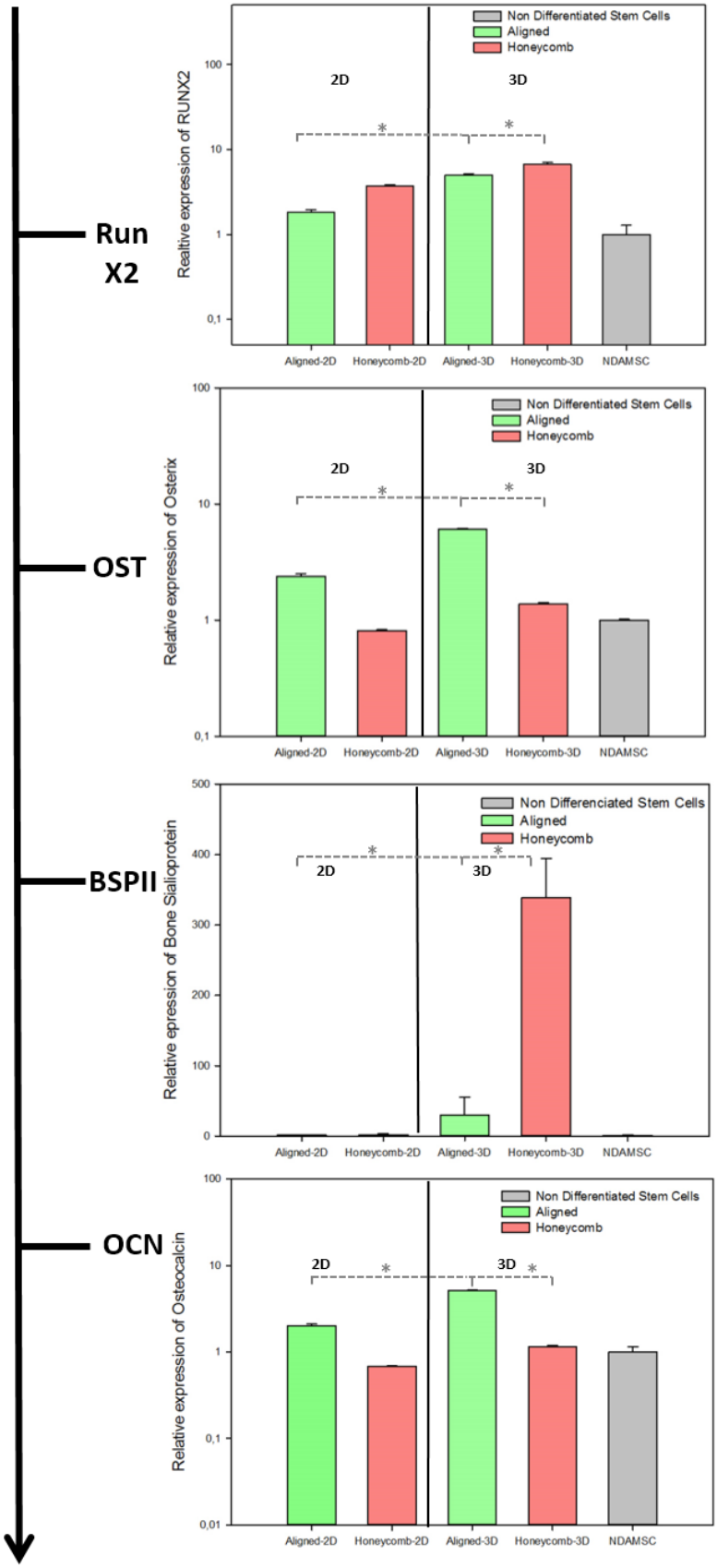
Run X2
Realtive expression of RUNX2
Non Differentiated Stem Cells
Aligned
Honeycomb
2D
3D
Aligned-2D
Honeycomb-2D
Aligned-3D
Honeycomb-3D
NDAMSC
OST
Relative expression of Osterix
BSPII
Relative epression of Bone Sialioprotein
Non Differenciated Stem Cells
OCN
Relative expression of Osteocalcin

Figure 3. Gene expression on the considered 2D and 3D constructs.

Relative expression of RUNX2, OSTERIX, BSPII, and OCN gene of ADMSC cultured for 21 days in osteogenic medium on 2D and 3D constructs different architectures (i.e., aligned and honeycomb). The symbol * denotes a statistically significant difference (i.e., $p < 0.05$).